# Multiwalled Carbon Nanotube Supported PtRu for the Anode of Direct Methanol Fuel Cells

**J. Prabhuram,[†] T. S. Zhao,*[,†] Z. K. Tang,[‡] R. Chen,[†] and Z. X. Liang[†]**

*Departments of Mechanical Engineering and Physics, The Hong Kong University of Science and Technology, Clear Water Bay, Kowloon, Hong Kong SAR, China*

*Received: November 19, 2005; In Final Form: January 22, 2006*

The activity of the methanol oxidation reaction of a multiwalled carbon nanotube (MWCNT)-supported PtRu catalyst was investigated and compared with the Vulcan XC-72 carbon-supported catalyst. The PtRu nanoparticles with 1:1 and 7:3 atomic ratios (with similar PtRu loadings and morphological structures) were deposited both on the MWCNTs and on the carbon. Cyclicvoltammetry results demonstrated that the MWCNT-supported PtRu catalyst exhibited a higher mass activity (mA $mg^{-1}$ of PtRu) for the methanol oxidation reaction than the carbon-supported PtRu under the condition that both catalysts possess more or less the same PtRu loadings, particle sizes, dispersions, and electrochemical surface area. The direct methanol fuel cell performance test data showed that MWCNT-supported PtRu catalysts yielded about 35−39% higher power densities than the carbon-supported PtRu.

## Introduction

Direct methanol fuel cells (DMFCs) are one of the potential power sources for portable electronic devices. However, challenging issues such as the poor kinetics of methanol oxidation reactions in the anode and methanol crossover from anode to cathode remain as the main obstacles in the development of DMFCs for commercial applications.[1−7] On the issue of improving the kinetics of the methanol oxidation reaction in the anode of a DMFC, generally, the Pt catalyst is alloyed with Ru and impregnated/deposited over conductive supports such as carbon powder, carbon blacks, carbon nanofibers, carbon nanotubes, and fullerene soot.[8−10] Furthermore, the activity of the methanol oxidation reaction can be essentially determined by the type of Pt crystallites present on the carbon supporting materials and also on the nature of interaction of the Pt particles with the carbon support.[11] It is interesting to mention that Bessel and co-workers[11c] showed that the methanol oxidation current for 5 wt % of Pt on graphite nanofibers was equivalent that of 25 wt % of Pt loading on Vulcan XC-72 carbon support. Although the crystalline nature of Pt particles on different types of carbon substrates has not been clearly established in previous works, the possibility for the occurrence of different types of Pt crystallite phases on carbon supporting materials such as carbon black and carbon nanofibers can be realized by means of rendering a substantially higher methanol oxidation current by carbon-nanofiber-supported Pt when compared to carbon-black-supported Pt.[11c] Following this investigation, many researchers have shown a considerable interest in using carbon nanotubes and carbon nanofibers as the supporting materials for PtRu in the anode of a DMFC, because of their unique structural, electrical, and mechanical properties.[12] For example, Steigerwalt et al.[13] employed bimetallic PtRu on different types of carbon supporting materials such as single-walled carbon nanotubes (SWCNTs), multiwalled carbon nanotubes (MWCNTs), and graphite carbon nanofibers (GCNFs), having either wide herringbone or narrow tubular herringbone atomic structures for the anode of a DMFC. They showed that the tubular herringbone GCNF yielded the highest DMFC performance among all other supporting materials. In their subsequent study,[10b] they also compared the DMFC performance for the PtRu-deposited GCNF anode with that of the unsupported PtRu colloid of similar surface area and particle size. It has been shown that the PtRu/GCNF yielded a 50% increase in cell performance compared to that of the unsupported PtRu colloid. In an another study, Park et al.[11c] showed that the PtRu supported on a carbon nanocoil exhibited higher methanol oxidation current than the PtRu supported on the Vulcan XC-72 carbon. In a similar fashion, the $PtWO_3$ catalytic particles dispersed on the carbon nanotubes gave higher methanol oxidation current due to better utilization of catalytic particles on the carbon nanotubes.[14] From these studies, it is understood that the atomic structure of the carbon supports is a crucial factor in influencing the catalytic activity of Pt or PtRu toward the methanol oxidation reaction.

In this work, to gain a better understanding of the influence of the atomic structure of different carbon supports on the catalytic activity of PtRu toward the methanol oxidation reaction, we have employed the most widely used carbon substrate materials, such as Vulcan XC-72 carbon and MWCNTs, as the supporting materials for the PtRu catalysts, and the activity of the methanol oxidation reaction of these catalysts was systematically investigated for the anode of a DMFC. The electrochemical measurements have shown that the MWCNT-supported PtRu exhibited a higher mass activity (mA $mg^{-1}$ of PtRu) for the methanol oxidation reaction than that of the carbon-supported PtRu under the condition that both catalysts possess similar PtRu loadings, particle sizes, dispersions, and electrochemical surface areas (ECSAs). The DMFC performance test showed that the power density yielded using the MWCNT-supported PtRu was 35−39% higher than that using the carbon-supported PtRu.

* Author to whom correspondence should be addressed. Phone: (852) 2358 8647. E-mail: metzhao@ust.hk.
[†] Department of Mechanical Engineering.
[‡] Department of Physics.

10.1021/jp0567063 CCC: $33.50 
Published on Web 02/22/2006

## Experimental Section

**Materials.** All of the chemicals used were of analytical grade. Hexachloroplatinic acid, ruthenium trichloride, sodium borohydride, tetraoctylammonium bromide (TOAB), nickel nitrate, and lanthanum nitrate were purchased from Aldrich. Tetrahydrofuran (THF), methanol, ethanol, and citric acid (all from Fischer Scientific Company) were used as received. Sulfuric acid and nitric acid were obtained from Merk. MWCNTs with diameters ranging from 40 to 60 nm and lengths ranging from 10 to 40 $\mu$m were prepared. Vulcan XC-72 carbon (particle size 30−50 nm) was procured from E-TEK Company. Polytetrafluroethylene (PTFE) and 5 wt % Nafion solution were received from Dupont and were used as received. High purity oxygen (99.999%), nitrogen (99.9%), carbon monoxide (99.9% purity), argon (99.9% purity), and methane gas were used in all of the experiments.

**Characterization Methods**. Transmission electron microscopy (TEM) images were obtained by using a high-resolution JEOL 2010 TEM system operating with a LaB6 filament at 200 kV. The samples were dispersed in ethanol under sonication and dropped on the carbon-coated grid and then imaged. The atomic compositions of the PtRu(1:1) and PtRu(7:3) nanoparticles supported on both the MWCNTs and the Vulcan XC-72 carbon were analyzed by an energy-dispersive X-ray (EDX) spectrometer, which was integrated with the TEM instrument. The X-ray diffraction (XRD) patterns of the Pt/C, Pt/MWCNT, PtRu/C, and PtRu/MWCNT nanocatalysts were obtained with a Philips powder diffraction system (model PW 1830) using a Cu K$\alpha$ source operating at 40 keV at a scan rate of 0.025° $s^{-1}$.

**Preparation, Purification, and Surface Oxidation of the MWCNTs**. The MWCNTs were prepared by means of the catalytic decomposition of $CH_4$ over Ni nanoparticles obtained from prereduced rare earth nickelate ($La_2NiO_4$). The $La_2NiO_4$ was first prepared by mixing an aqueous solution of $Ni(NO_3)_2 \cdot 6H_2O$ and $La(NO_3)_3 \cdot 6H_2O$ with the appropriate stoichiometry in 100% excess of citric acid. The resulting gel was evaporated at 80 °C with stirring until viscous syrup was formed. The obtained residue was calcined in air at 500 °C for 4 h and then pelleted prior to calcination at 800 °C for 6 h. The prepared catalyst $La_2NiO_4$ was placed in a quartz boat, which was inserted into a horizontal quartz glass reactor. Initially, $La_2NiO_4$ was reduced in a flow of $H_2$ (20 mL/min) from room temperature to 800 °C and kept at this temperature for 0.5 h. Then, the reactor temperature was lowered to 700 °C for the in situ reaction. After the reactor was swept with Ar gas, $CH_4$ was introduced into the reactor, passing over the catalyst at flow rate of 30 mL/min for 60 min. After being cooled to ambient temperature in a flow of Ar, the MWCNTs were collected. The carbon residue was washed using deionized (DI) water until the pH value of solution was close to 7 and dried at 300 °C in a flow of Ar. Further, purification was carried out by refluxing MWCNTs with 60% $HNO_3$ at 90 °C for 2 h to remove the metal particles. Afterward, the mixture was diluted with water, filtered, washed with excess DI deionized (DI) water, and dried at 50 °C in a vacuum oven for overnight. After the purification process, the surface oxidation of the MWCNTs was carried out by refluxing MWCNTs in 4 M $H_2SO_4$ + 4 M $HNO_3$ at 90 °C for 5 h. Finally, the treated MWCNTs were diluted with water, filtered, washed with excess DI water, and dried at 50 °C in a vacuum oven overnight.

**Preparation of PtRu Nanoparticles on the MWCNTs and on the Vulcan XC-72 Carbon**. The PtRu nanoparticles with different atomic compositions, 1:1 and 7:3, supported both on the MWCNTs and on the Vulcan XC-72 carbon were prepared by using $NaBH_4$ as a reducing agent with the surfactant TOAB. The PtRu/MWCNT and PtRu/C nanocatalysts at 20 wt % were prepared by maintaining a constant concentration of TOAB (0.87 mM) with $H_2PtCl_6$ (0.0065 mM) and $RuCl_3 \cdot 6H_2O$ (0.0065 mM) in a THF solvent. An appropriate amount of the precursor solutions with TOAB and the supporting materials, either MWCNTs (surface treated) or carbon, were taken in a THF solvent. The resulting suspensions were stirred for 2 h, and then the solvent THF was evaporated at 60 °C. After complete evaporation of the solvent, the dry mixtures were dispersed in diluted methanol and ultrsonicated for 15 min. Subsequently, an excess quantity of 0.15 M $NaBH_4$ was added, drop-by-drop, to the mixtures with vigorous stirring for the complete reduction of Pt and Ru from their respective metal salts. After that, the mixtures were stirred for 2 h at room temperature. Finally, the mixtures were filtered, washed with excess DI water, and dried in a vacuum oven at 70 °C for 2 h. For comparison, we also prepared Pt nanoparticles (20 wt %) supported both on the MWCNTs and on the carbon by the above method. To remove the TOAB from the surface of the Pt and PtRu nanoparticles supported on the MWCNTs and on the carbon, all of the catalytic powders were dispersed in ethanol and ultrsonicated for 15 min. Then, they were centrifuged in excess ethanol at a speed of 15000 rpm for 10 min, and the treated ethanol was siphoned off. This centrifugation process was repeated five times. Finally, all of the catalysts were dried in a vacuum oven at 70 °C for 2 h to remove the trace amount of alcohol.

**Preparation of the Working Electrode**. Glassy carbon (GC) (Taizhou Electroanalytical Instrument Factory, China, 4 mm diameter, 0.125 $cm^2$) was polished to a mirror finish with 0.05 $\mu$m alumina suspension before each experiment and served as an underlying substrate of the working electrode. The catalyst ink was prepared by ultrasonically dispersing 7.2 mg of 20 wt % of Pt/C, Pt/MWCNT, PtRu/C, and PtRu/MWCNT in 2.5 mL of ethanol, to which 0.5 mL of 0.1 wt % Nafion solution was added, and the dispersion was ultrasonicated for 30 min. A quantity of 10 $\mu$L of the dispersion was pipetted out on the top of the GC and over which 10 $\mu$L of 0.1 wt % Nafion was added. Then, the electrode was dried at 70 °C to yield a PtRu loading of 48 $\mu$g $cm^{-2}$.

**Preparation of the Membrane Electrode Assembly.** Commercial Nafion 115 membranes (Electrochem, Inc.) were treated according to the standard membrane cleaning procedure.[15] Briefly, the Nafion 115 membranes were boiled at 80 °C for 1 h in 5% $H_2O_2$ solution, DI water, and 0.5 M $H_2SO_4$ solution and again in DI water. Finally, the membranes were air-dried. For fabrication of the anode, commercial-grade 30 wt % Teflon-treated carbon cloth (E-TEK) was employed as the backing layer. The gas diffusion layers (GDLs) were fabricated on one side of the carbon cloth comprising Vulcan XC-72 carbon and 20 wt % Teflon. To fabricate anode catalyst layers, the anode inks were prepared by mixing in-house-made 20 wt % PtRu-(1:1) and PtRu(7:3) supported on the MWCNTs and on the Vulcan XC-72 carbon with 30 wt % Nafion solution in a 2-propanol solvent. The prepared anode inks were uniformly brushed on the GDL in a 1 $cm^2$ area to give an approximate loading of 2.1 mg $cm^{-2}$ of PtRu on the anode. Finally, 0.5 mg $cm^{-2}$ of Nafion was uniformly coated on the anode catalyst layers and dried at 80 °C in a vacuum oven for 30 min. The commercial E-TEK Pt/C (40 wt % metal with 2 mg of Pt $cm^{-2}$) catalyst was used as the cathode. The membrane electrode assembly was formed by sandwiching the Nafion 115 membrane between the anode and the cathode and by hot pressing it at 135 °C under a pressure of 4 MPa for 3 min.

**Electrochemical Measurements**. Electrochemical measurements were carried out by cyclicvoltammetry (CV) using a potentiostat (EG&G Princeton, model 273A). A conventional, three-electrode cell consisting of GC with an area of 0.125 $cm^2$ as the working electrode, Pt wire as the counter electrode, and a saturated calomel electrode (SCE) as the reference electrode was used. The reference electrode was placed in a separate chamber, which is located near the working electrode through a Luggin capillary tube. The CV experiments were performed in 0.5 M $H_2SO_4$ solution containing 1 M $CH_3OH$ at a scan rate of 50 mV $s^{-1}$. All of the solutions were prepared by using ultrapure water (Millipore, 18 MΩ). $N_2$ gas was purged for nearly 30 min before starting the experiment. In all of the experiments, stable voltammogram curves were recorded after scanning for 10 cycles in the potential region from −0.24 to 1.0 V in 0.5 M $H_2SO_4$ solution. The chronoamperometry (current vs time response) tests were conducted using a three-electrode cell in 0.5 M $H_2SO_4$ solution containing 1 M $CH_3OH$ at 0.6 V for a period of 3000 s. The CO stripping voltammogram was conducted with a three-electrode cell in 0.5 M $H_2SO_4$ solution. Initially, an $N_2$ gas was purged to 0.5 M $H_2SO_4$ solution for 30 min. Afterward, the CO gas was purged from the 0.5 M $H_2SO_4$ solution for 30 min by maintaining the electrode potential at −0.18 to −0.16 V vs SCE at a scan rate of 0.5 mV $min^{-1}$. Then, the dissolved CO in the solution was removed by bubbling nitrogen gas into the solution for 30 min. Finally, the stripping voltammograms were collected between −0.18 and 1.0 V with a scan rate of 50 mV $s^{-1}$ under $N_2$.

**Direct Methanol Fuel Cell Performance Test**. The MEAs fabricated by using the MWCNT-supported PtRu and carbon-supported PtRu catalysts at the anode were tested in a single-cell fixture (with an active area of 1 $cm^2$) having three-pass serpentine flow channels with both widths and depths of 0.7 mm. The MEAs were initially activated at 70 °C for 20 h by feeding 1 M methanol at a flow rate of 1 mL $min^{-1}$ to the anode and dry oxygen gas at a flow rate of 10 mL $min^{-1}$ to the cathode. After the activation process, the DMFC performance curves were obtained at 70 °C by feeding 2 M methanol at a flow rate of 1 mL $min^{-1}$ using a high-pressure piston pump (model series III, Scientific Systems, Inc.) and by purging dry oxygen gas into the cathode at a flow rate of 10 mL $min^{-1}$ at ambient pressure. Performance curves were recorded by fixing the load current, which was controlled with an electric load system (BT2000, Arbin Instrument, Inc.).

## Results and Discussion

**Physicochemical Characterization of PtRu Particles on the MWCNTs and on the Vulcan XC-72 Carbon.** Figure 1 shows the XRD patterns of the Pt and PtRu particles with atomic ratios of 7:3 and 1:1 deposited on the MWCNTs and on the carbon. The XRD patterns of Pt/C and Pt/MWCNT catalysts exhibited diffraction peaks of (111), (200), (220), and (311) at 2$\theta$ values of 39.9°, 46.3°, 67.45°, and 81.9°, respectively. These peaks indicate that Pt was present in the face-centered cubic (fcc) structure. The PtRu(7:3)/C, PtRu(7:3)/MWCNT, PtRu(1:1)/C, and PtRu(1:1)/MWCNT catalysts displayed diffraction patterns similar to those of the Pt, except the 2$\theta$ values were shifted to higher values. This has indicated that single-phase PtRu was formed both on the carbon and on the MWCNTs. It is interesting to note that the extent of shifting of 2$\theta$ values is found to be increased with increasing the Ru content in the catalysts. For instance, the 2$\theta$ values of the (111) peaks for the PtRu(7:3)/C and PtRu(7:3)/MWCNT are observed at 40.6° and 40.3° whereas, for the PtRu(1:1)/C and PtRu(1:1)/MWCNT, the 2$\theta$ values of the (111) peaks are slightly shifted to higher values, 41.0° and 40.75°, respectively. This may indicate the formation of a higher degree of alloy for the PtRu with an atomic ratio 1:1 both on the carbon and on the MWCNTs.[16] Furthermore, on comparison of the shift in 2$\theta$ values among the PtRu/C and PtRu/MWCNT catalysts, the PtRu/C with 7:3 and 1:1 atomic ratios exhibited a higher shift in 2$\theta$ values than the PtRu/MWCNT with atomic ratios of 7:3 and 1:1, indicating the formation of a higher degree of alloy for the PtRu/C than the PtRu/MWCNT. The peaks associated with a typical hexagonal close-packed (hcp) structure of pure Ru and $RuO_2$ did not appear in the XRD pattern of PtRu/C and PtRu/MWCNT, suggesting the absence of metallic Ru and its oxides in the PtRu alloy. Although the peaks associated with pure Ru and $RuO_2$ are not present in the pattern, the presence of some amount of metallic Ru and its oxides in the amorphous state is always possible,[17] especially on the MWCNTs, because of the formation of a relatively lower degree of PtRu alloy on them. The relatively more broad type of diffraction peaks for the PtRu present on the carbon might indicate the amorphous nature of the PtRu particles and their good interaction with the carbon support.[16b] Furthermore, the existence of sharp diffraction peaks (002) around a 2$\theta$ value at 26° demonstrates the crystalline nature of MWCNTs.[11c,18] Hence, MWCNTs can act as a good conductive substrate and influence the crystalline nature of the Pt and PtRu particles being dispersed over them. In the case of carbon, at the same 2$\theta$ value very broad peaks appeared, which indicate the amorphous nature of the Vulcan XC-72 carbon. The average particle sizes for the PtRu/MWCNTs and PtRu/C catalysts was calculated from the broadening of the (220) diffraction peaks using Scherrer's equation[19]

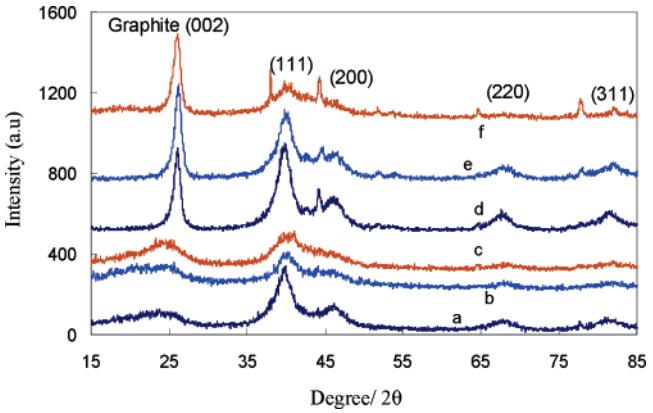


**Figure 1.** XRD patterns of (a) Pt/C, (b) PtRu(7:3)/C, (c) PtRu(1:1)/C, (d) Pt/MWCNTs, (e) PtRu(7:3)/MWCNTs, and (f) PtRu(1:1)/MWCNTs.

$$d = \frac{0.9\lambda}{B_{2\theta} \cos \theta_{max}} \quad (1)$$

where $\lambda$ is the wavelength of the X-ray (1.54056 Å), $\theta$ is the angle at the maximum of the peak, and $B_{2\theta}$ is the width of the peak at half-height.

In the preparative process of the PtRu catalysts, all of the parameters were maintained in an identical way to ensure that the loading, dispersions, and sizes of the PtRu particles were essentially the same both on the carbon and on the MWCNTs. Figure 2 shows the TEM images for the PtRu(1:1)/C, PtRu(7:3)/C, PtRu(1:1)/MWCNT, and PtRu(7:3)/MWCNT catalysts. It can be seen from this figure that in all the catalysts the PtRu particles of sizes around 3−4 nm with more or less uniform dispersions were formed on both the Vulcan XC-72 carbon and the MWCNTs. The mean particle sizes calculated from the TEM

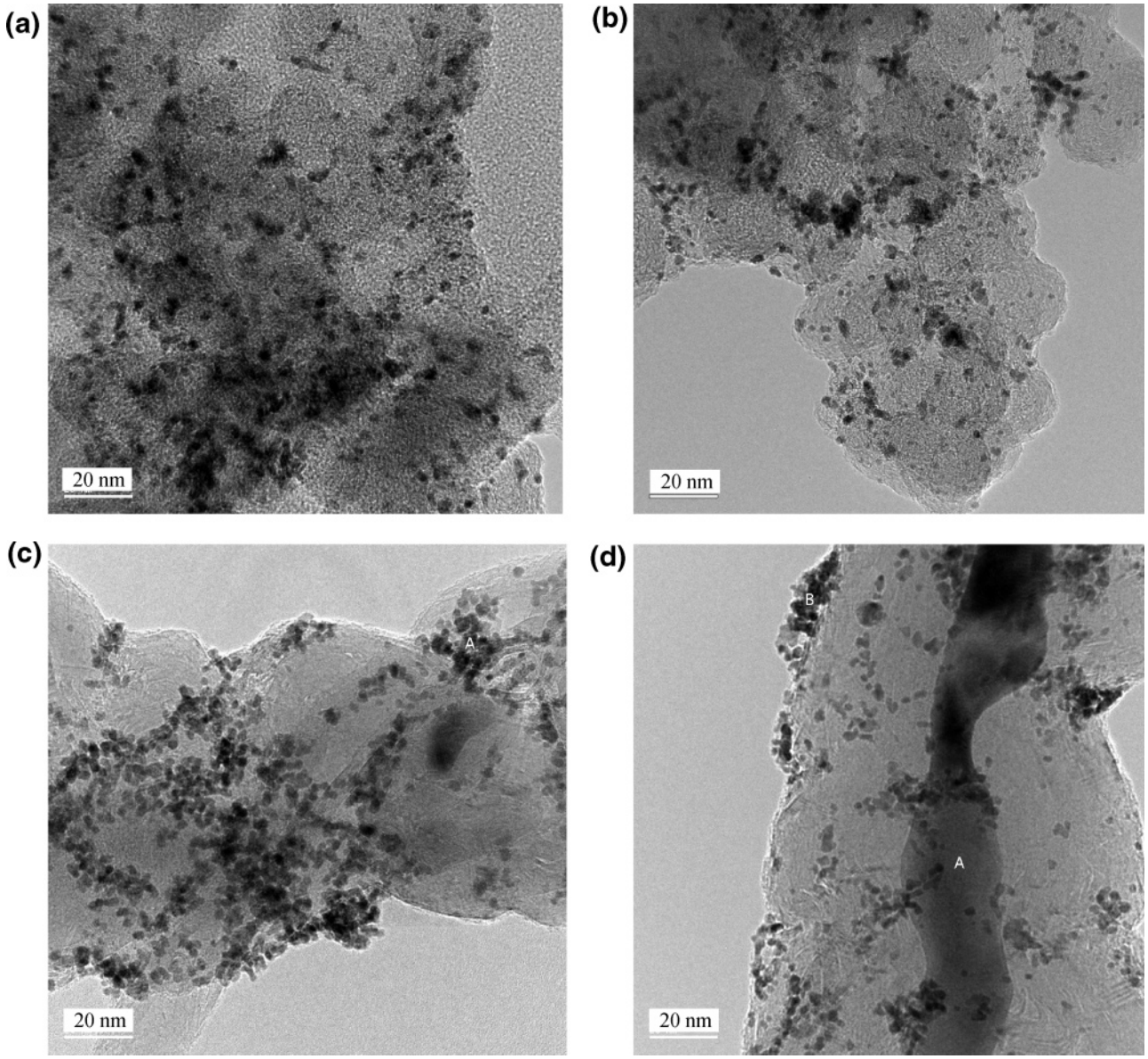


**Figure 2.** TEM images of (a) PtRu(1:1)/C, (b) PtRu(7:3)/C, (c) PtRu(1:1)/MWCNTs and (d) PtRu(7:3)/MWCNTs.

**TABLE 1: Mean Particle Sizes and Atomic Compositions of Pt and Ru Obtained from EDX Analysis**

| nominal atomic composition (%) | particle size from TEM (nm) | particle size from XRD (nm) | Pt atom (%) | Ru atom (%) |
|---|---|---|---|---|
| MWCNT/PtRu (50:50) | 3.2 | 2.8 | 49.09 | 50.91 |
| MWCNT/PtRu (70:30) | 3.1 | 2.3 | 70.81 | 29.19 |
| C/PtRu (50:50) | 3.3 | 2.7 | 51.67 | 48.33 |
| C/PtRu (70:30) | 3.2 | 2.6 | 73.37 | 26.63 |

images were found to be consistent with the average particle sizes calculated from XRD peak widths, which are given in Table 1. In some parts of the TEM images, an aggregation of particles was observed. This is because in this work we have adopted a new method for the preparation of PtRu nanoparticles, which needs to be improved further to obtain very uniform dispersion on the substrate materials. Additionally, it appears from the TEM images that the PtRu particles have a better interaction with the Vulcan XC-72 carbon support than with the MWCNTs. This is probably due to the availability of more surface area of the former, which can facilitate better dispersion of the particles than on the latter.[11c] This might be the reason for the relatively broad nature of XRD peaks for the PtRu particles dispersed on the carbon as discussed in the previous section.

The TEM-EDX analysis was also conducted by focusing the electron beam on several different selected individual PtRu particles for each sample of the PtRu with atomic ratios of 1:1 and 7:3 both on the carbon and on the MWCNTs. The atomic compositions of Pt and Ru present in different individual particles are in close agreement with nominal atomic composition of the catalysts and are given in Table 1. This gives further evidence for the formation of single-phase PtRu both on the MWCNTs and on the carbon.

**Electrochemical Characterization of Pt and PtRu Nanoparticles on MWCNTs and Vulcan XC-72 Carbon**. As discussed in the Introduction, the electro-oxidation of methanol solely depends on the types of the Pt crystallite phases present on the carbon supporting materials. Thus, to understand the nature of the Pt crystallite phases present both on the MWCNTs and on the Vulcan XC-72 carbon, which can be roughly characterized by the hydrogen adsorption/desorption profiles of the CV,[11a,20] we have conducted CV studies for the Pt particles present on the MWCNTs and on the carbon in the supporting electrolyte in the absence of methanol. Figure 3 shows the

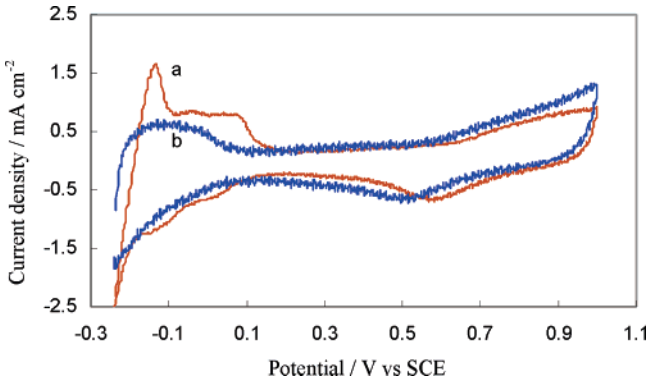


**Figure 3.** CV curves of (a) Pt/MWCNTs and (b) Pt/C in 0.5 M $H_2SO_4$ solution.

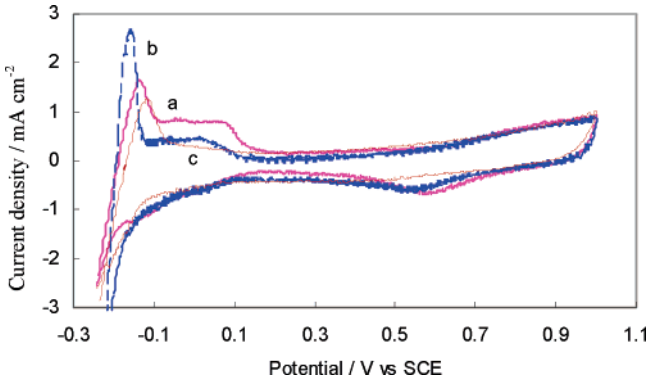


**Figure 4.** CV curves of (a) Pt/MWCNTs, (b) PtRu(7:3)/MWCNTs, and (c) PtRu(1:1)/MWCNTs in 0.5 M $H_2SO_4$ solution.

stabilized CV curves recorded for the 20 wt % Pt/MWCNT (curve a) and 20 wt % Pt/C (curve b) in 0.5 M $H_2SO_4$ in the potential ranging from −0.24 to 1.0 V. For the Pt/MWCNT catalyst, two broad peaks occur in the potential ranging from −0.08 to 0.14 V, followed by a sharp hydrogen desorption peak centered at −0.15 V. The formation of a sharp hydrogen desorption peak at −0.15 V can be due to the predominance of the Pt(110) crystallite phase in the Pt particles present on the surface of the MWCNTs, which is in close agreement with the data reported in the literature.[9,10,11a,20] However, in the case of the Pt/C catalyst, although the hydrogen desorption peak was poorly resolved, one can observe a very broad peak in the potential region from −0.24 to 0.08 V. The formation of a broad type of hydrogen desorption peak for the Pt/C in 0.5 M $H_2SO_4$ electrolyte agrees well with our recently reported data.[21] This can be attributed to the predominance of the Pt(111) crystallite phase in the Pt particles present on the carbon support.[11a,20] Furthermore, in the cathodic sweep, a monolayer oxide ($PtO_x$) reduction peak potential difference of nearly 100 mV has been noted between the Pt/MWCNT and Pt/C catalysts. This can reflect the potential difference in the formation of the monolayer oxide during the anodic sweep for the two distinct Pt crystallite phases present on the MWCNTs and on the carbon as discussed above.

Figure 4 shows the CV curves recorded for the 20 wt % Pt (curve a), PtRu(7:3) (curve b), and PtRu(1:1) (curve c) supported on the MWCNTs in 0.5 M $H_2SO_4$ in the potential ranging from −0.24 to 1.0 V. As discussed in the preceding section, for the Pt/MWCNT catalyst, two broad hydrogen desorption peaks occur in the potential region from −0.08 to 0.14 V, followed by a sharp hydrogen desorption peak centered at −0.15 V. In the case of PtRu(7:3), only a single and broad hydrogen desorption peak with less magnitude is formed in the potential ranging from −0.11 to 0.12 V, followed by a sharp peak at −0.16 V. Interestingly, for the PtRu(1:1), the broad hydrogen desorption peak followed by the sharp peak at −0.11 V was completely suppressed (curve c). This is because increasing the Ru concentration in the PtRu catalyst (as in the 1:1 atomic ratio) can easily dissociate the water molecules in the lower potential region starting from −0.11 V, and the resultant $OH^-$ ions produced by the dissociation of water can adsorb on the Ru atoms and form ruthenium hydrous oxide species. The formation of these species at the lower potential of −0.11 V can suppress the hydrogen desorption peak occurring on the Pt atoms.[22] Furthermore, the double-layer charging current is found to be increasing with an increasing amount of Ru in the catalyst. The observed results for the PtRu catalysts with atomic ratios of 1:1 and 7:3 on the MWCNTs are consistent with the data reported in the literature.[10] The CV results further confirmed the fact that the bimetallic PtRu existed in a single phase on the surfaces of the MWCNTs.

**CO Stripping Voltammetry**. To compare the ECSA for the PtRu particles present both on the MWCNTs and on the Vulcan XC-72 carbon, we have conducted CO stripping voltammetry for all of the catalysts. Figure 5 shows the CO stripping voltammograms and the subsequent CV curves for the PtRu-(1:1)/C (Figure 5a), PtRu(1:1)/MWCNT (Figure 5b), PtRu(7:3)/C (Figure 5c), and PtRu(7:3)/MWCNT (Figure 5d) in 0.5 M $H_2SO_4$ solution. It can be observed from the figure that for all the PtRu catalysts the hydrogen desorption peaks are completely suppressed in the lower potential region, which is due to the saturated coverage of $CO_{ads}$ species on the Pt sites of these catalysts.[23] For the PtRu(1:1) and PtRu(7:3) supported on the carbon, the onset of CO oxidation takes place at 0.35 and 0.33 V, respectively. Although there is a slight difference in the onset of the CO oxidation potential between these two catalysts, these values are consistent with the data reported in the literature.[24,25] In the case of PtRu(1:1)/C, two broad CO oxidation current peaks appeared in the potential ranging from 0.35 to 1.0 V, whereas for the PtRu(7:3)/C a broad CO oxidation peak followed by a small peak was observed in the potential ranging from 0.33 to 1.0 V. Also, for the PtRu(1:1) and PtRu(7:3) supported on the MWCNTs, a similar type of two broad CO oxidation current peaks was observed. However, the difference between the onset potentials of CO oxidation for these two catalysts is found to be high (90 mV). The cause for this big difference in the onset potential of CO oxidation is not understood at this moment. It has to be noted that for the PtRu(1:1) and PtRu(7:3) supported on the carbon the upper potential limit for the CO oxidation peak was not clearly determined, because these peaks merged with the monolayer oxide formation peaks. The formation of two broad CO oxidation peaks almost in all of the catalysts can be attributed to the presence of heterogeneous phases of PtRu, Ru, and $RuO_x$ on the surface of the PtRu catalysts as discussed in the XRD section,[22,24] and detailed discussion of this phenomenon is beyond the scope of the present work.

We measured the ECSA for all the catalysts by using the CO oxidation charge after subtracting the background current of the subsequent CV curves in 0.5 M $H_2SO_4$ solution with the assumption of 420 $\mu$C cm$^{-2}$ as the oxidation charge for one monolayer of CO on a smooth Pt surface. We could obtain only an approximate CO oxidation charge, particularly for the PtRu-(1:1) and PtRu(7:3) supported on the carbon because of the nonavailability of a clear upper potential limit for the CO oxidation peak as mentioned above. Under this circumstance, the CO oxidation charge was arbitrarily measured up to the

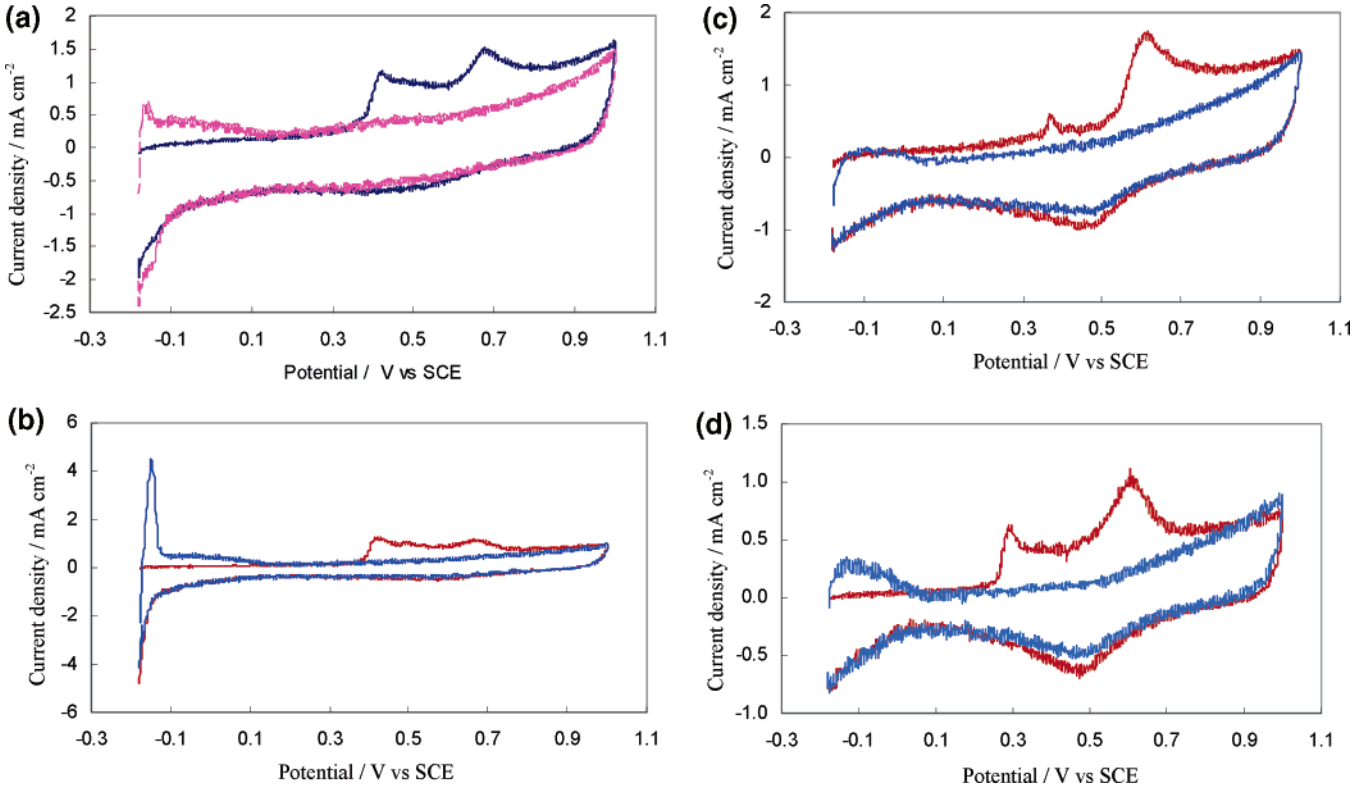


**Figure 5.** CO stripping voltammogram and the subsequent CV curves of (a) PtRu(1:1)/C, (b) PtRu(1:1)/MWCNTs, (c) PtRu(7:3)/C, and (d) PtRu(7:3)/MWCNTs in 0.5 M $H_2SO_4$ solution.

**TABLE 2: Catalyst Loading, ECSA, and Mass Activity for Methanol Oxidation for the PtRu/C and PtRu/MWCNT Catalysts**

| catalyst | PtRu loading ($\mu$g cm$^{-2}$) | ECSA (m$^2$ g$^{-1}$) | mass activity at 0.7 V (mA mg$^{-1}$) |
|---|---|---|---|
| PtRu(1:1)/MWCNTs | 48 | 93.0 | 175 |
| PtRu(1:1)/C | 48 | 99.5 | 125 |
| PtRu(7:3)/MWCNTs | 48 | 83.3 | 115 |
| PtRu(7:3)/C | 48 | 97.6 | 75 |

upper potential limits of 0.80 and 0.75 V, where the downfall of the second CO oxidation peaks ended for PtRu(1:1)/C and PtRu(7:3)/C, respectively (Figures 5a and 5c). The measured ECSA values are given in Table 2. Table 2 shows that the ECSA values for the PtRu present both on the MWCNTs and on the carbon are found to be more or less similar.

**Evaluation of Methanol Electro-Oxidation**. Figure 6 shows the CV curves recorded for the PtRu(1:1)/MWCNT, PtRu(1:1)/C, PtRu(7:3)/MWCNT, and PtRu(7:3)/C in 0.5 M $H_2SO_4$ solution with 1 M $CH_3OH$ in the potential range from −0.18 to 1.0 V. The methanol oxidation current was normalized to the amount of PtRu loading on the MWCNTs and on the carbon. For the PtRu(1:1) supported both on the MWCNTs and on the carbon, the onset of the methanol oxidation reaction takes place at 0.38 V. However, the MWCNT-supported PtRu(1:1) exhibited a higher methanol oxidation current when compared to the carbon-supported PtRu(1:1). A similar trend was also noted for the PtRu(7:3) supported both on the MWCNTs and on the carbon. The mass activity of the methanol oxidation reaction at 0.7 V was compared for all of the PtRu catalysts and is given in Table 2. Similarly, we have observed a higher mass activity for the methanol oxidation reaction for the MWCNT-supported Pt than that of the carbon-supported Pt (data not shown). As discussed in the CV results of the Pt catalysts in the supporting electrolyte (Figure 3), the predominance of the Pt(110) crystallite phase on the MWCNTs (as identified from the hydrogen

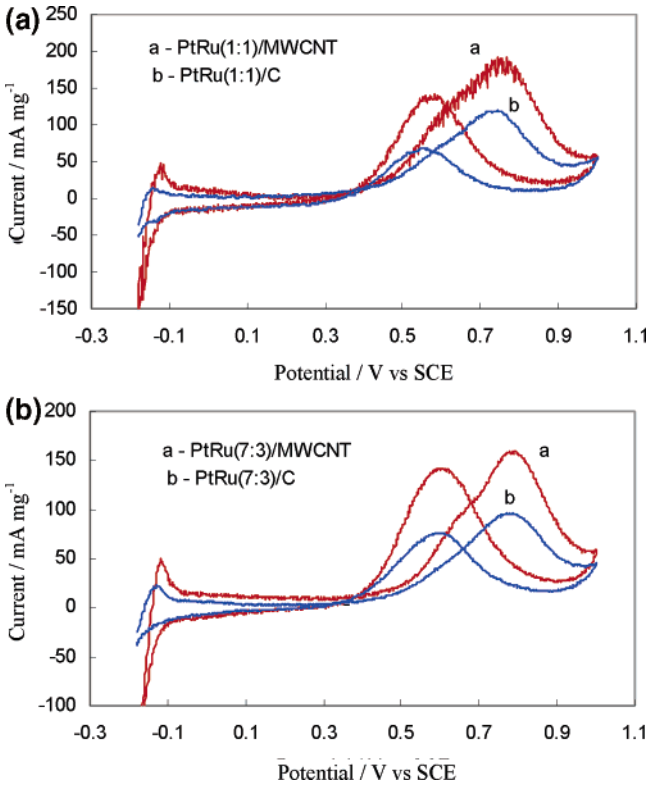


**Figure 6.** CV curves of (a) PtRu(1:1) supported on the MWCNTs and carbon and (b) PtRu(7:3) supported on the MWCNTs and carbon in 0.5 M $H_2SO_4$ + 1 M $CH_3OH$.

adsorption/desorption profiles), which is regarded as the highly active phase for methanol oxidation reaction, is likely to be the reason for the enhanced methanol oxidation reaction for the Pt and PtRu particles supported on the MWCNTs.[11a] Some of the previous investigations,[13,26] which compared the methanol

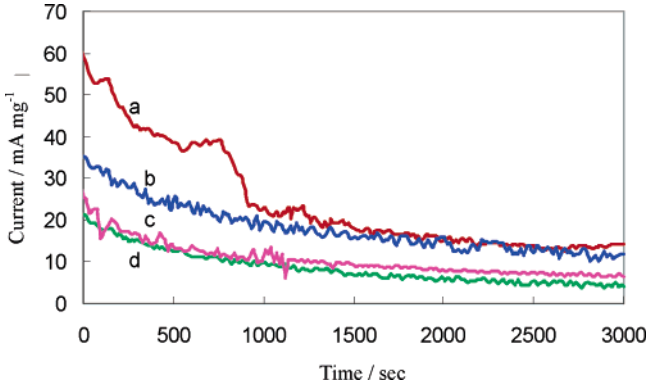


**Figure 7.** Chronoamperometry curves for (a) PtRu(1:1)/MWCNTs, (b) PtRu(1:1)/C, (c) PtRu(7:3)/MWCNTs, and (d) PtRu(7:3)/C in 0.5 M $H_2SO_4$ + 1 M $CH_3OH$.

oxidation reaction on the Pt and PtRu particles supported on the different carbon substrates also showed the higher methanol oxidation current for the Pt and PtRu particles supported on the SWCNTs and on the MWCNTs. They attributed that the higher electrochemical surface area and higher electronic conductivity of the SWCNTs and MWCNTs can be the decisive factors in enhancing the catalytic activity of Pt and PtRu particles toward the methanol oxidation reaction. Although these reasons hold for the enhancement of the methanol oxidation reaction, the present study gives the impetus that the probable existence of a distinctive crystallite phase, i.e., Pt(110), of the Pt particles on the conductive walls of the MWCNTs might also be an additional factor in enhancing the activity of the methanol oxidation reaction. Earlier, although Bessel and co-workers had emphasized this point through their work,[11c] a detailed investigation would be required to identify the different crystallite phases of the Pt nanoparticles supported on different carbon substrates and their influence on the methanol oxidation reaction. Additionally, the presence of a relatively higher amount of nonalloyed Ru in the PtRu/MWCNT catalyst might also participate in enhancing the methanol oxidation reaction through the bifunctional mechanism.

Further, to compare the long-term performance of the PtRu particles on the MWCNTs and on the carbon toward the methanol oxidation reaction, we have conducted chronoamperometry tests in 0.5 M $H_2SO_4$ solution containing methanol for 3000 s. Figure 7 shows the chronoamperometry curves for the PtRu(1:1)/MWCNT, PtRu(1:1)/C, PtRu(7:3)/MWCNT, and PtRu(7:3)/C in 0.5 M $H_2SO_4$ + 1 M $CH_3OH$ at the constant potential of 0.6 V. In the initial period of time, the potentiostatic current decreases rapidly for all the PtRu catalysts, which can be due to the formation intermediate species, such as $CO_{ads}$, $CH_3OH_{ads}$, and $CHO_{ads}$, during the methanol oxidation reaction.[27] However, the close observation of the chronamperometry curves revealed that potentiostatic current decreases very rapidly for the PtRu(1:1) supported on the MWCNTs. This might be due to the higher deactivation of the Pt(110) crystallite phase (the probable Pt crystallite phase of the PtRu particles present on the surface of MWCNTs) by the $CO_{ads}$ species during the methanol oxidation reaction.[11a] At long times, although the current gradually decays for all the catalysts, the MWCNT-supported PtRu catalysts maintained a slightly higher current than the carbon-supported PtRu. The long time decay can be attributed to the adsorbed anion $SO_4^{2-}$ on the surface of the catalysts, which can restrict the methanol oxidation reaction.[23]

**Direct Methanol Fuel Cell Performance Test**. The catalytic performance of the PtRu nanoparticles supported on the MWCNTs and on the Vulcan XC-72 carbon was compared in a practical DMFC system. Figure 8 compares the performance of the DMFC anode using the 20 wt % PtRu(1:1)/MWCNT, PtRu(1:1)/C, PtRu(7:3)/MWCNT, and PtRu(7:3)/C nanocatalysts with 2 M methanol at 70°C under the same testing conditions. The PtRu(1:1) and PtRu(7:3) supported on the MWCNTs showed higher open circuit voltage (OCV) and performance throughout the entire current density regions than the PtRu(1:1) and PtRu(7:3) supported on the carbon. The PtRu(1:1) supported on the MWCNTs yielded a power density of 32 mW $cm^{-2}$, which is about 35% higher than that of the PtRu(1:1) supported on the carbon (21 mW $cm^{-2}$). Similarly, the PtRu(7:3) supported on the MWCNTs yielded a power density that is around 39% higher than that of the PtRu(7:3) supported on the carbon. Among the PtRu(1:1) and PtRu(7:3) supported on the MWCNTs, the former catalyst yielded higher performance than the latter, which is consistent with the mass activity data obtained from the CV studies. Further improvement of the morphology of the PtRu catalyst on the surface of the MWCNTs can enhance the cell performance to a greater extent.

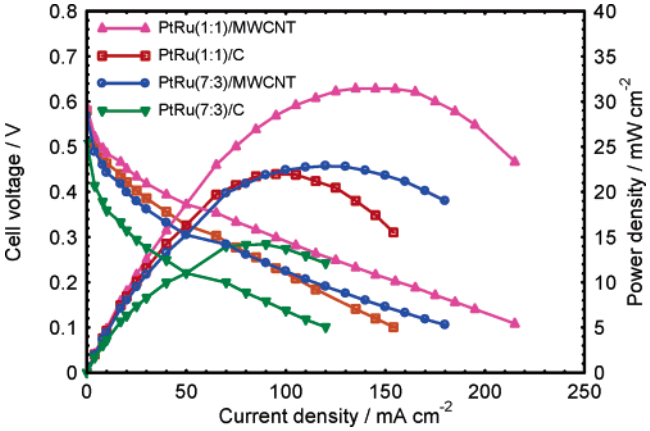


**Figure 8.** Comparison of DMFC performance using MWCNT-supported PtRu and carbon-supported PtRu catalysts at the anode with 2 M methanol at 70 °C.

## Conclusions

In the present work, to study the influence of carbon supporting materials on the PtRu catalyst toward the methanol oxidation reaction, two different carbon substrates such as MWCNTs and Vulcan XC-72 carbon were employed as the supporting materials for the PtRu particles with atomic ratios of 1:1 and 7:3. The morphological properties of the MWCNT-supported PtRu and carbon-supported PtRu catalysts were evaluated by the TEM and XRD data, and it is found that well-dispersed small PtRu particles (3−4 nm) with a single phase were formed on these two supporting materials. The CO stripping voltammogram results indicated that the PtRu supported both on the MWCNTs and on the carbon have more or less similar ECSAs. Interestingly, the CV results demonstrated that the MWCNT-supported PtRu catalyst exhibited a higher mass activity (mA $mg^{-1}$ of PtRu) for the methanol oxidation reaction than that of the carbon-supported PtRu. Although we have not provided any concrete evidence for the presence of different Pt crystallite phases on the MWCNTs and on the carbon, it is believed from these findings that the existence of the distinctive Pt crystallite phases, i.e., Pt(110), on the PtRu particles supported on the MWCNTs is likely to be reason for enhancing the activity of the methanol oxidation reaction. Finally, the DMFC performance test data showed that PtRu(1:1) and PtRu(7:3) supported on the MWCNTs yielded power

densities that are about 35% and 39% higher than those of PtRu-(1:1) and PtRu(7:3) supported on the carbon, respectively.

**Acknowledgment.** The work described in this paper was supported by grants from the Research Grants Council (Project Nos. 622305 and 605003).

## References and Notes

(1) Wasmus, S.; Kuver, A. *J. Electroanal. Chem.* **1999**, *461* (1−2), 14.

(2) Ren, X. Zelenay, P.; Thomas, S.; Davey, J.; Gottesfeld, S. *J. Power Sources* **2000**, *86* (1−2), 11.

(3) Prabhuram, J.; Zhao, T. S.; Liang, Z. X.; Yang, H. Wong, C. W. *J. Electrochem. Soc.* **2005**, *152* (7), A1390.

(4) Ye, Q.; Zhao, T. S.; Yang, H.; Prabhuram, J. *Electrochem. Solid-State Lett.* **2005**, *8* (1), A52.

(5) Prabhuram, J.; Zhao, T. S.; Yang, H. *J. Electroanal. Chem.* **2005**, *578*, 105.

(6) Liu, J. G.; Zhao, T. S.; Chen, R.; Wong, C. W. *Electrochem. Commun.* **2005**, *7*, 288.

(7) Yang, H.; Zhao, T. S.; Ye, Q. *Electrochem. Commun.* **2004**, *6*, 1098.

(8) Hills, C. W.; Nashner, M. S.; Frenkel, A. I.; Shapely, J. R.; Nuzzo, R. G. *Langmuir* **1999**, *15*, 690.

(9) Che, G.; Lakshmi, B. B.; Fisher E. R.; Martin, C. R. *Nature* **1998**, *393*, 346.

(10) Che, G.; Lakshmi, B. B.; Martin, C. R.; Fisher, E. R. *Langmuir* **1999**, *15*, 750.

(11) (a) Herrero, E.; Franasazczuk, K.; Wieckowski, A. *J. Phys. Chem.* **1994**, *98*, 5074. (b) Augustine, R. L. *Heterogeneous Catalysis for the Synthetic Chemist*; Marcel Dekker: New York, 1996; p 170. (c) Bessel, C. A.; Laubernds, K.; Rodriguez, N. M.; Baker, R. T. K. *J. Phys. Chem. B* **2001**, *105*, 1115. (d) Park, K. W.; Sung, Y. E.; Han, S.; Yun, Y.; Hyeon, T. *J. Phys. Chem. B* **2004**, *108*, 939.

(12) (a) Iijima, S. *Nature* **1991**, *354*, 56. (b) Ebbesen, T. W.; Lezec, H. J.; Hiura, H.; Bennett, J. W.; Ghaemi, H. F.; Thio, T. *Nature* **1996**, *384*, 54. (c) Dai, H.; Hafner, J. H.; Rinzler, A. G.; Colbert, D. T.; Smalley, R. *Nature* **1996**, *384*, 147.

(13) (a) Steigerwalt, E. S.; Deluga, G. A.; Lukehart, C. M. *J. Phys. Chem. B* **2002**, *106*, 760. (b) Steigerwalt, E. S.; Deluga, G. A.; Cliffel, D. E.; Lukehart, C. M. *J. Phys. Chem. B* **2001**, *105*, 8097.

(14) (a) Rajesh, B.; Thampi, K. R.; Bonard, J. M.; Xanthopoulos, N.; Mathieu, H. J.; Viswanathan, B. *J. Phys. Chem. B* **2003**, *107*, 2701. (b) Rajesh, B.; Karthik, V.; Karthikeyan, S.; Thampi, K. R.; Bonard, J. M.; Viswanathan, B. *Fuel* **2002**, *81*, 2002.

(15) Weng, D.; Wainright, J. S.; Landau, U.; Savinell, R. F. *J. Electrochem. Soc.* **1996**, *143*, 1260.

(16) Shukla, A. K.; Arico, A. S.; El-Khatib, K. M.; Kim, H.; Antonucci, P. L.; Antonucci, V. *Appl. Surf. Sci.* **1999**, *137*, 20.

(17) (a) Yang, B.; Lu, Q.; Wang, Y.; Zhaung, L.; Lu, J.; Liu, P.; Wang, J.; Wang, R. *Chem. Mater.* **2003**, *15*, 3552. (b) Antolini, E.; Cardellini, F. *J. Alloys Compd.* **2001**, *315*, 118. (c) Antolini, E.; Cardellini, F.; Giorgi, L. *J. Mater. Sci. Lett.* **2000**, *19*, 2099. (d) Roth, C.; Martz, N.; Fuess, H. *Phys. Chem. Chem. Phys.* **2001**, *3*, 315. (e) Roth, C.; Martz, N.; Morlang, A.; Theissmann, R.; Fuess, H. *Phys. Chem. Chem. Phys.* **2004**, *6*, 3557.

(18) Li, W.; Liang, C.; Zhou, W.; Qiu, J.; Zhou, Z.; Sun, G.; Xin, Q. *J. Phys. Chem. B* **2003**, *107*, 6292.

(19) Gojkovic, S. L.; Vidakovic, T. R.; Durovic, D. R. *Electrochim. Acta* **2003**, *48*, 3607.

(20) Markovic, N.; Gasteiger, H.; Ross, P. N. *J. Electrochem. Soc.* **1997**, *144*, 1591.

(21) Prabhuram, J.; Wang, X.; Hui, C. L.; Hsing, I.-M. *J. Phys. Chem. B* **2003**, *107*, 11057.

(22) Lee, C. E.; Bergens, S. H. *J. Phys. Chem. B* **1998**, *102*, 193.

(23) Jiang, J.; Kucernak, J. *J. Electranal. Chem.* **2003**, *543*, 187.

(24) Crabb, E. M.; Ravikumar, M. K.; Thompsett, D.; Hurford, M.; Rose, A.; Russell, A. E. *Phys. Chem. Chem. Phys.* **2004**, *6*, 1792.

(25) Guo, J. W. Zhao, T. S.; Prabhuram, J.; Chen, R.; Wong, C. W. *Electrochim. Acta* **2005**, *51*, 754.

(26) (a) Carmo, M.; Paganin, V. A.; Rosolen, J. M.; Gonzalez, E. R. *J. Power Sources* **2005**, *142*, 169. (b) Huang, J. E.; Guo, D. J.; Yao, Y. G.; Li, H. L. *J. Electroanal. Chem.* **2005**, *577*, 93. (c) Wu, G.; Chen, Y S.; Xu, B. Q. *Electrochem. Commun.* **2005**, *7*, 1237.

(27) Kabbabi, A.; Faure, R.; Durand, R.; Beden, B.; Hahn, F.; Leger, J.-M.; Lamy, C. *J. Electroanal. Chem.* **1998**, *444*, 41.